frontiers | Frontiers in Built Environment

TYPE Original Research
PUBLISHED 26 November 2024
DOI 10.3389/fbuil.2024.1443587

OPEN ACCESS

EDITED BY
Abdullah Mohsen Zeyad,
Jazan University, Saudi Arabia

REVIEWED BY
Jue Li,
Chongqing Jiaotong University, China
Xinzhou Li,
Chang'an University, China

*CORRESPONDENCE
Hao Liang,
lianghao@sdjtky.cn

RECEIVED 04 June 2024
ACCEPTED 04 November 2024
PUBLISHED 26 November 2024

CITATION
Zhou K, Liang H, Huang F and Cheng Z (2024) Evaluation for anti-cracking performance of polyurethane grout based on overlay test. *Front. Built Environ.* 10:1443587. doi: 10.3389/fbuil.2024.1443587

Evaluation for anti-cracking performance of polyurethane grout based on overlay test

Kun Zhou[1], Hao Liang[2]*, Feiheng Huang[3] and Ziqing Cheng[3]

[1]Shandong Hi-speed Construction Management Group Co., Ltd, Jinan, China, [2]Key Laboratory for Road Structure and Material of Shandong Province, Shandong Transportation Institute, Jinan, China, [3]Shandong Expressway Peninsula Investment Co., Ltd, Jinan, China

Polyurethane grouting has garnered increasing attention in road maintenance, owing to its exceptional interfacial adhesion, mechanical robustness, and chemical resilience. In comparison to conventional SBS-modified asphalt, polyurethane grout offers superior durability and demonstrates an enhanced capacity to inhibit crack propagation within asphalt mixtures. This study investigates the anti-cracking performance of polyurethane grout in comparison to traditional SBS-modified asphalt, utilizing the Overlay Test (OT) to simulate real-world conditions of reflective cracking in asphalt pavements. Results demonstrate that polyurethane grout significantly enhances the crack resistance of asphalt mixtures, manifesting superior durability and resistance to crack propagation at a controlled temperature of 25°C, with a marked increase in the number of loading cycles relative to the control. However, the performance of polyurethane grout is notably diminished under adverse conditions of low temperatures and water immersion. The investigation employs a multi-index evaluation, with gray correlation analysis delineating the efficacy of various indices in appraising crack resistance. Recommending the use of loading cycles, allowable failure times, and cumulative fracture energy as key metrics.

KEYWORDS

polyurethane grout, reflective cracking resistance, overlay test, grey correlation analysis, pavement maintenance

1 Introduction

Reflective cracking of asphalt concrete overlays remains a pervasive and detrimental pavement distress in semi-rigid base asphalt pavement structures. Extensive research efforts have been devoted to address the issue of reflective cracking in both laboratory and field settings. Chen (2019) and Qian et al. (2018) utilized MTS test equipment and numerical simulation to study the fatigue crack resistance of geotextiles, revealing their effectiveness in mitigating reflective cracking through reduced crack propagation rate and width. Fang et al. (2023) examined crack control through base layer strength enhancement using strength testing and field compaction experiments. Shen et al. (2021) evaluated the crack resistance of basalt fiber grids using impact resilience and dynamic fatigue testing, demonstrating their ability to improve the fracture toughness and fatigue resistance of asphalt mixtures. Pan (2019) analyzed the stress re-laxation effects of SAK warm mix rubberized asphalt and SBS polymer modified asphalt using ANSYS finite element modeling, elucidating the excellent cracking resistance and reflective cracking prevention capacity of warm mix rubberized asphalt in cold regions. Wang et al. (2016) applied discrete element modeling and multilayered base model to investigate the damage mechanisms and internal structural

factors influencing the effectiveness of large stone porous mixtures (LSPM) in mitigating reflective cracking in semi-rigid bases, revealing the effectiveness of crack propagation delay and stress concentration release of LSPM. Hu (2021) studied the stress response of asphalt overlay composite pavements using finite element analysis to develop an optimized model for reflective crack analysis and explored the effects of crack-resistant layers through fatigue loading experiments. Hu (2019) extensively researched the anti-cracking performance of basalt fiber-reinforced cement-stabilized aggregate bases, proposing the use of basalt fiber strips to effectively reduce reflective cracking and enhance material durability. Su and Zhu. (2022) analyzed the stress response and reflective cracking mechanisms of ultra-thin asphalt overlays on old concrete pavements, establishing a combined active-passive anti-reflective cracking structure and validating its effectiveness through mechanical simulations and real-world measurements. In summary, current reflective cracking research focuses primarily on preventive measures implemented during the design and construction of new pavements to retard reflective cracking initiation through base layer optimization and fracture resistance enhancements. While beneficial for new pavements, effective remediation techniques for existing pavements with evident reflective cracking remain understudied. Considering that initiated reflective cracks perpetuate and expand to other areas, severely compromising ride quality and safety while reducing overall pavement strength and service life, developing economical and practical repair solutions to extend the lifespan of existing pavements holds tremendous practical significance for ensuring roadway durability and prolonging maintenance cycles.

Polyurethane grouting technology has emerged as a novel trenchless remediation method for latent defects in asphalt pavements, garnering increasing attention in the field of road maintenance in recent years. Previous studies (Gao et al., 2017; Zhang et al., 2017; Jiang et al., 2022; Li et al., 2017) have demonstrated numerous superior performance characteristics of polyurethane compared to conventional asphalt materials, including (1) low viscosity and high permeability, (2) high consolidation strength and outstanding mechanical properties, (3) rapid chemical reaction without curing requirements, and (4) excellent engineering adaptability and operability. Thus, polyurethane grouting is regarded as an efficacious technology capable of mitigating reflective cracks in practical applications for both road maintenance and pre-overlaying distress treatment. Consequently, experimental investigations into the anti-reflective cracking performance of polyurethane have progressively been conducted from various perspectives. Wang et al. (2019) examined the mechanical response of polyurethane aggregate composites under axial loading, finding that mixture brittleness and strength increase with density, while overall system compressive performance is minimally correlated with density. Wang (2018) characterized the mechanical properties of fractured rock formations reinforced by a new water glass/polyurethane grout, establishing a three-dimensional damage creep model based on experimental results to evaluate the effectiveness of the grouting reinforcement. Xu W et al. (2024) demonstrated that high-strength polyurethane composite (HSPUC) significantly enhances the structural integrity of concrete, effectively reinforcing the material by delaying crack propagation and improving both stiffness and load-bearing capacity. Liu et al. (2018) conducted a comprehensive study on the reinforcement properties of fractured structural surfaces based on surface roughness, analyzing the variation patterns of mesoscopic fractured surface shear strength.

Most previous studies have focused predominantly on assessing anti-cracking performance through dynamic testing of composite specimens under various stress conditions. Conventional tests often apply constant stress or strain to examine only the crack initiation phase, without including the propagation stage. The loading methods and boundary constraints employed in these experiments diverge from the natural development of reflective cracks, resulting in test results that may have limited applicability or realism (Braun et al., 2022; Xu C C et al., 2024).

The Overlay Test (OT) captures both the initiation and propagation phases of cracking, closely mirroring real-world conditions and yielding a more comprehensive dataset (Gu et al., 2015). Using OT, Zhai et al. (2017) analyzed the fracture resistance of large stone porous mixture (LSPM), finding that the number of load cycles (***N***) and maximum load loss rate (***R***) could fully characterize the cracking resistance. Wei et al. (2021) investigated the influence of different test factors on the fracture resistance and behavior of large stone asphalt mixtures, finding that the energy needed for crack propagation exceeded that for initiation, with fracture energy somewhat increasing as temperatures fell. Walubita et al. (2021) analyzed correlations between OT data and reflective cracking performance of in-service highways, demonstrating the OT's utility as a repeatable laboratory test for evaluating the cracking potential of hot mix asphalt compared to field performance. In summary, Overlay Test has seen moderate use as a more effective evaluation method for simulating reflective cracking, offering enhanced realism compared to other laboratory tests.

Current research on the grouts has concentrated largely on analyzing the mechanical properties of grout-aggregate composites from a holistic structural perspective, but direct evaluations of the crack resistance of grouting materials remain limited. In this paper, Overlay Test (OT) was utilized to conduct an extensive evaluation of the anti-reflective cracking capabilities of polyurethane grouting material. The evaluation was carried out under various temperature conditions as well as after aging treatments to simulate real-world pavement environments. Through this approach, the study focused on assessing key performance indicators including crack initiation, propagation behavior, cumulative fracture energy, and load-bearing capacity to quantify the material's effectiveness in resisting reflective cracking. The results demonstrate that polyurethane grouting material significantly delays crack propagation and enhances resistance to reflective cracking, particularly in aged and temperature-variable conditions, offering a promising insight into the optimization of pavement maintenance strategies and emphasizing the practical applications of polyurethane grouts in enhancing roadway durability.

2 Materials and methods

2.1 Materials

Research materials included SBS modified asphalt and polyurethane grout, which were all synthesized in the laboratory.

TABLE 1 Technical indexes of SBS-modified asphalts.

Test item	Penetration 25°C (0.1 mm)	Ductility 5°C (cm)	Softening point (°C)	Viscosity 135°C (Pa.s)	RTFOT		
					Residual Penetration	Residual Ductility	Residual SP
SBS	49	30	78	1.8	42	19	72

TABLE 2 Raw material information of PU.

Main agents			Additives				
Polyether Polyol	Polyester Polyol	Isocyanate	Foam Stabilizer	Flame Retardant	Latent Curing Agent	Chain Extender	Cross-link Agent
Polyoxypropylene triol	Phthalic anhydride	PAPI	Dimethicone	Tripoly--phosphate	Silane Terminated Polyurethane	Butanediol	Pentaerythritol

Given our research aim to evaluate the effectiveness and efficiency of these materials in addressing pavement cracking, SBS modified asphalt was used as a control to compare with the bonding performance of the polyurethane grout. This comparison is intended to reveal the potential advantages and limitations of polyurethane in practical applications, thereby providing a more comprehensive reference for pavement repair and material selection.

2.1.1 SBS asphalt preparation

To produce the SBS modified asphalt, the Shell 70# asphalt binder was first heated to at least 160°C to ensure optimal fluidity. Subsequently, at temperatures between 170°C and 180°C, appropriate amounts of SBS and extracted oil were added sequentially under a shear rate of 4,000 rpm, with a 45-min shearing process. Finally, stabilizers were introduced at 180°C under a mixing rate of 700 rpm, followed by 150 min of low-speed blending. Below are the technical indexes of this SBS modified material (Table 1).

2.1.2 Polyurethane grout preparation

Regardless of the specific application, polyurethane's structure comprises soft and hard segments, with the soft segments primarily derived from polyols and the hard segments from the carbamate formed by the reaction of isocyanate and alcohol hydroxyl group (Liu, 2019). The balance and composition of these segments dictate the material properties of the polyurethane. Polyether and polyester polyols are the most commonly used soft segment monomers. Polyether polyols offer superior thermal resistance, whereas polyester polyols excel in mechanical strength and impact resistance. Isocyanates, classified as either aromatic or aliphatic, further influence the properties of polyurethane. Aromatic isocyanates, characterized by the presence of benzene rings, enhance mechanical strength but tend to exhibit poor resistance environmental factors, while aliphatic isocyanates provide better overall weatherability but offering lower mechanical performance. Therefore, considering the intended application scenario and the desired performance, the following raw materials were selected (Table 2).

The polyurethane grout was synthesized using the well-established one-step method, a widely adopted approach in industrial polyurethane production for its straightforward procedure and broad applicability. Following this method, the grout was produced through a three-step process, ensuring both reliability and consistency with standard practices in the field. Firstly, a quantity of polyols and chain extender were added to a reaction vessel heated to 110°C and dehydrated under vacuum for 1 hour. Secondly, foam stabilizer, latent curing agent, cross-link agent, and flame retardant were introduced in set ratios after cooling to 50°C and mixed for 1 hour, yielding a composite polyether material. Finally, a 1.2:1 mass ratio mixture of the composite polyether and polymeric diphenylmethane diisocyanate (PAPI) was rapidly stirred to obtain the final polyurethane material. Upon the completion of synthesis, the material underwent thorough analysis to verify its structure and performance. The infrared spectrum is shown in Figure 1.

The FTIR analysis was conducted over a wavenumber range of 500–4,000 cm^{-1}, with 16 scans at a resolution of 4 cm^{-1}. As shown in Figure 1, the characteristic peak at 1721 cm^{-1} corresponds to the stretching vibration of the carbonyl group (C = O), which is key evidence of the formation of urethane bonds, indicating the successful reaction between the isocyanate and polyol to form polyurethane. Additionally, the N-H stretching vibration observed at 3,303 cm^{-1} further confirms the presence of urethane linkages. The absorption peak at 2,269 cm^{-1}, associated with the isocyanate group (N = C = O), suggests the participation of isocyanates in the reaction, with the relatively weak intensity of this peak indicating only a small amount of residual isocyanate. The absorption peaks at 1,104 cm^{-1} and 1,224 cm^{-1} correspond to the stretching vibrations of C-O-C ether bonds, reflecting the presence of polyether polyol as the soft segment. Meanwhile, the peak at 1,598 cm^{-1} is attributed to the C = C stretching vibrations in the aromatic ring, derived from the aromatic isocyanate structure of PAPI in the polyurethane hard segment. These spectral features confirm a typical polyurethane material synthesis, of which

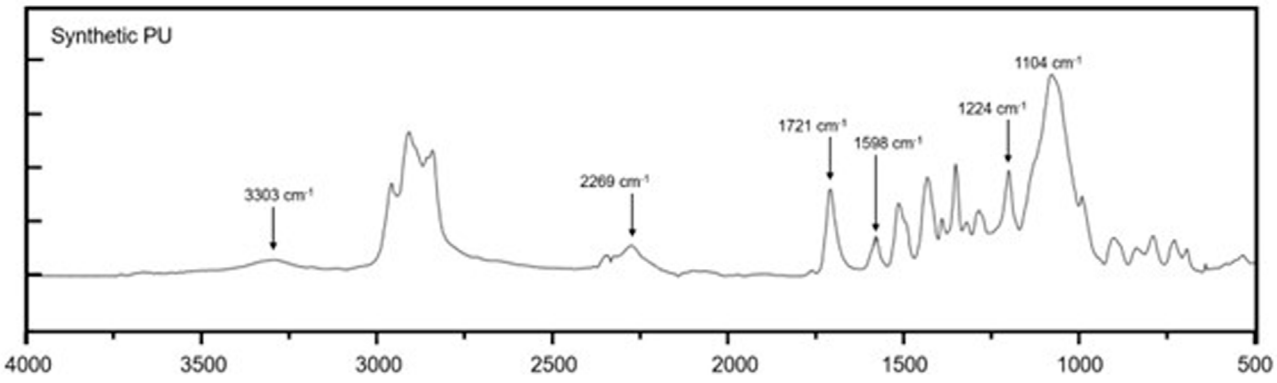

FIGURE 1
Infrared spectrum of PU material.

TABLE 3 Technical indexes of PU material.

No.	Test items		Values	Standard
1	Viscosity (25°C), mPa·s	A component	480	GB/T 12,009.3
		B component	617	GB/T 22,314
2	Density (25°C), g/cm^3	A component	1.26	GB/T 4472
		B component	1.2	GB/T 15,223
3	Solidify time, min		4 ~ 5	—
4	Expansion ratio		1.1 ~ 1.5	—
5	Dimensional stability (−30°C), %		−0.15, −0.35, −0.42	GB/T 8811
	Dimensional stability (80°C), %		1.06, 1.04, 1.22	
6	Compressive strength (25°C), MPa		10.5	GB/T 8813
7	Tensile strength (25°C), MPa		9.1	GB/T 1040.1
8	Anti-permeability (3 mm), MPa		>0.6	GB/T 328.10
9	Foaming state in water		Low expansion ratio with relatively hard texture	—
10	Chemical corrosion resistance	10% Sodium chloride solution	Insoluble	GB/T 11,547
		Lime suspension	Insoluble	
		5% Sulfuric acid	Insoluble	

possessing the essential structural characteristics and representative properties.

The technical indicators of the polyurethane grout material are present in Table 3.

A preliminary analysis of the performance indices for the aforementioned polyurethane grout indicates that the composites synthesized in the laboratory demonstrate notable mechanical strength. Specifically, the compressive and tensile strengths were recorded at 10.5 MPa and 9.1 MPa, respectively. In addition to this, the materials exhibit exceptional dimensional stability, undergoing minimal deformation in both high and low temperature conditions (less than 1.5% at high temperatures and under 0.5% at low temperatures). Significantly, the grout, when solidified in water, showed no signs of loosening, maintaining a glossy surface texture and a hard consistency. These characteristics establish a strong engineering foundation for the use of this material in the repair of reflective cracks in areas with high moisture, which is critical for practical engineering applications.

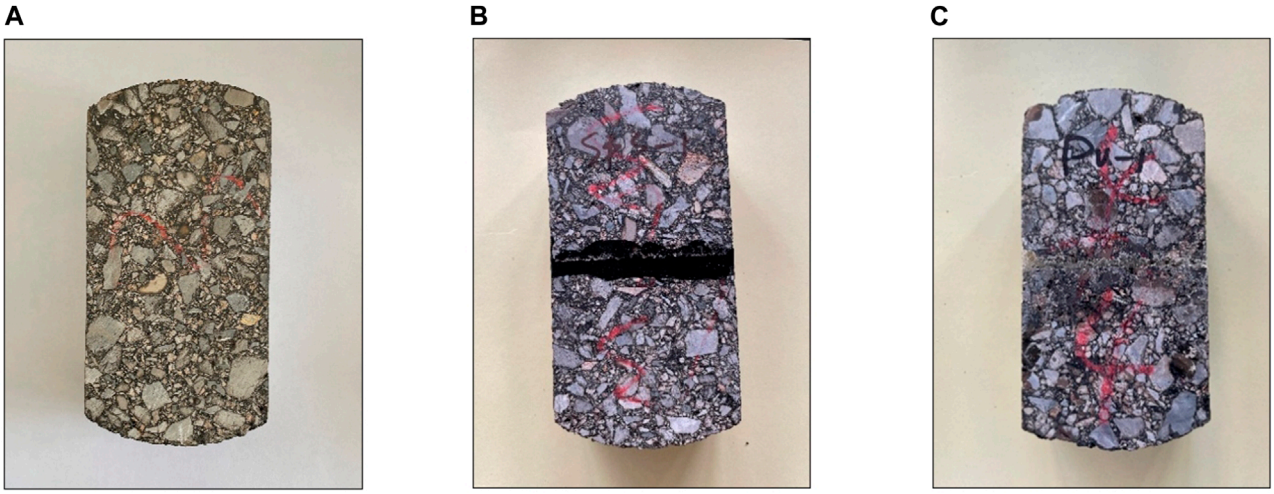

FIGURE 2
(A) Standard OT sample; **(B)** Bonding with SBS asphalt; **(C)** Bonding with polyurethane.

2.2 Methods

The methods employed in this study are designed to systematically assess the anti-cracking performance of polyurethane grout compared to traditional SBS-modified asphalt under various environmental conditions. Section details include specimen preparation, the specific testing protocols of the Overlay Test, and the comprehensive experimental procedures.

2.2.1 Specimen preparation

The preparation of OT specimen is as follows: (1) Prepared well-graded standard AC-13 SBS asphalt mixture Marshall specimen through gyratory compaction; (2) Carried out cutting process to shape Marshall specimen into standard OT sample according to its size requirements; (3) Divided all OT pieces into 3 groups: **first** group is used as blank control without any operation; specimens from **second** group were cut along the center and then bonded with SBS asphalt; the cutting operation of **third** group was consistent with the pervious one but the bonding materials become polyurethane grout instead. Specimens are shown in Figure 2.

2.2.2 Overlay test

Each specimen was attached to two tensile plates with epoxy resin adhesive and in-stalled on the test equipment, as shown in Figure 3.

There is a gap of 2–3 mm in the middle of the OT mold, with the left part tightly fixed and the right half capable of horizontal movement to produce a transverse displacement of 0.635 mm back and forth. The crack width of 2–3 mm is inherently determined by the base of the OT mold, in accordance with the specifications Tex-248-F (TxDOT, 2021). This crack width serves to effectively simulate the typical crack dimensions found in actual pavement conditions. Consequently, the use of this crack width ensures both the accuracy and the practical relevance of the experimental results. In this setup, this test simulates the crack opening and closing motion of reflection cracking under the conjoint action of temperature and load through multiple periodic displacement transformation which realized by a sine triangle wave loading mode. The end of this test is marked by a 93% loading loss rate (the load in one certain cycle/initial maximum load = 7%) or the completion of 1,200 cycles.

2.2.3 Indices and analytical method

According to the specification Tex-248-F and current research status (Zhai et al., 2018), the load loss rate (***R***), number of loading cycles (***N***), cumulative fracture energy (***G***), initial maximum load (***F***), allowable failure time (***J***), average fracture energy (G^*), and critical fracture energy (***Ec***) were used to evaluate the crack resistance performance of bonding materials under different conditions.

- Load loss rate (***R***);

R represents the load change in an asphalt mixture reflection crack from its initiation to penetration. After a crack form, repeated loads significantly accelerate the internal damage process of the asphalt mixture, directly indicating the attenuation in tensile stress during loading.

- Number of loading cycles (***N***);

N represents the number of cycles a specimen has endured before reaching a set load loss or fracture energy ratio. A higher value of N signifies improved crack resistance, allowing it to endure more vehicle loads and temperature changes without developing reflective cracks.

- Cumulative fracture energy (***G***);

Fracture energy is the energy needed for crack propagation per unit area when a specimen undergoes tensile loading. G represents

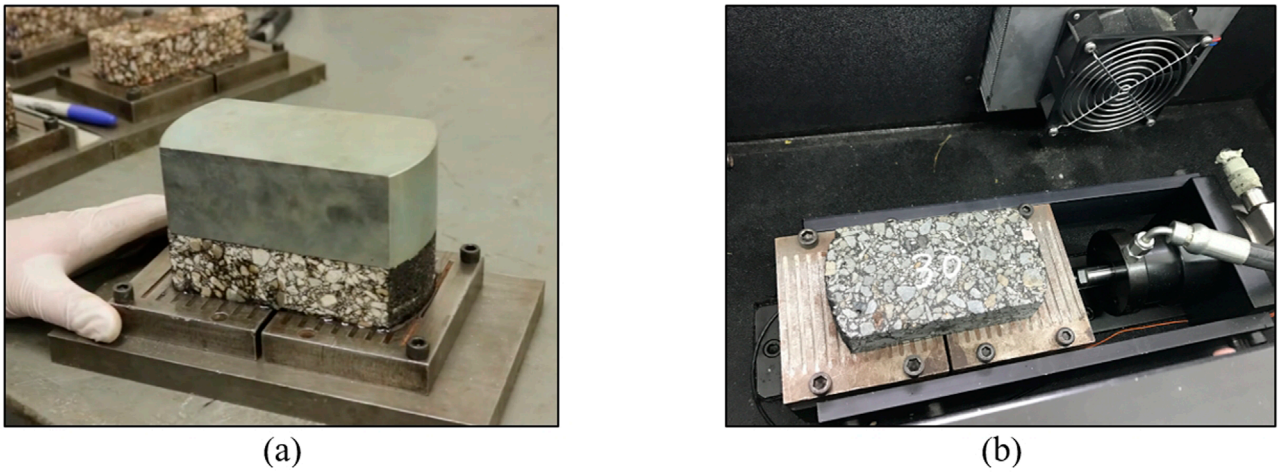

FIGURE 3
(A) OT sample; **(B)** OT equipment.

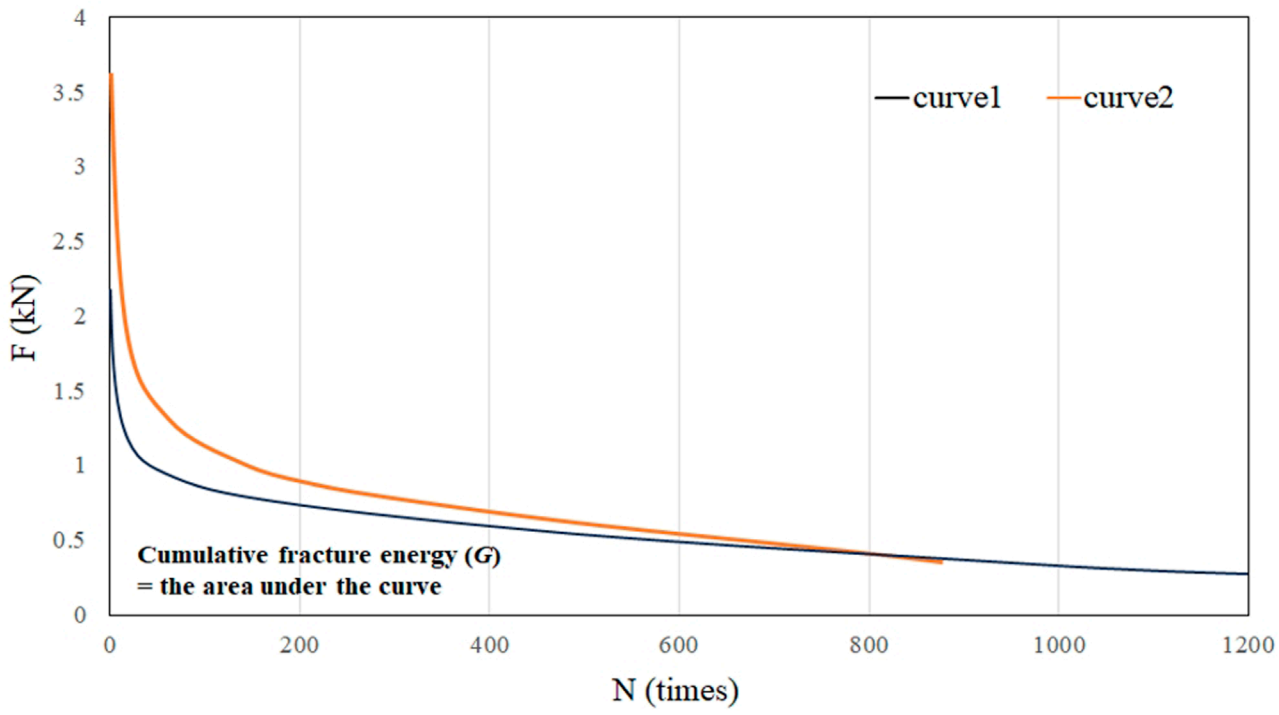

FIGURE 4
Two different scenarios in overlay test.

the total energy required from the start of loading until complete fracture failure, calculated as the area under the curve of the load period (Figure 4).

- Initial maximum load (***F***);

F refers to the maximum load reached by the specimen during the first loading cycle in the test.

- Allowable failure times (***J***);

Typically, the test terminates at ***R*** of 93% or ***N*** of 1,200. Figure 4 shows two typical specimen failure scenarios with similar ***G*** values and varying ***N*** values: curve 2 exhibits high initial load but ***R*** dropping to 93% before ***N*** reaches 1,200; curve 1 exhibits low initial load but ***R*** above 93% at the end of the test. To mitigate these effects, the ***J*** index was introduced by referencing fracture mechanics and

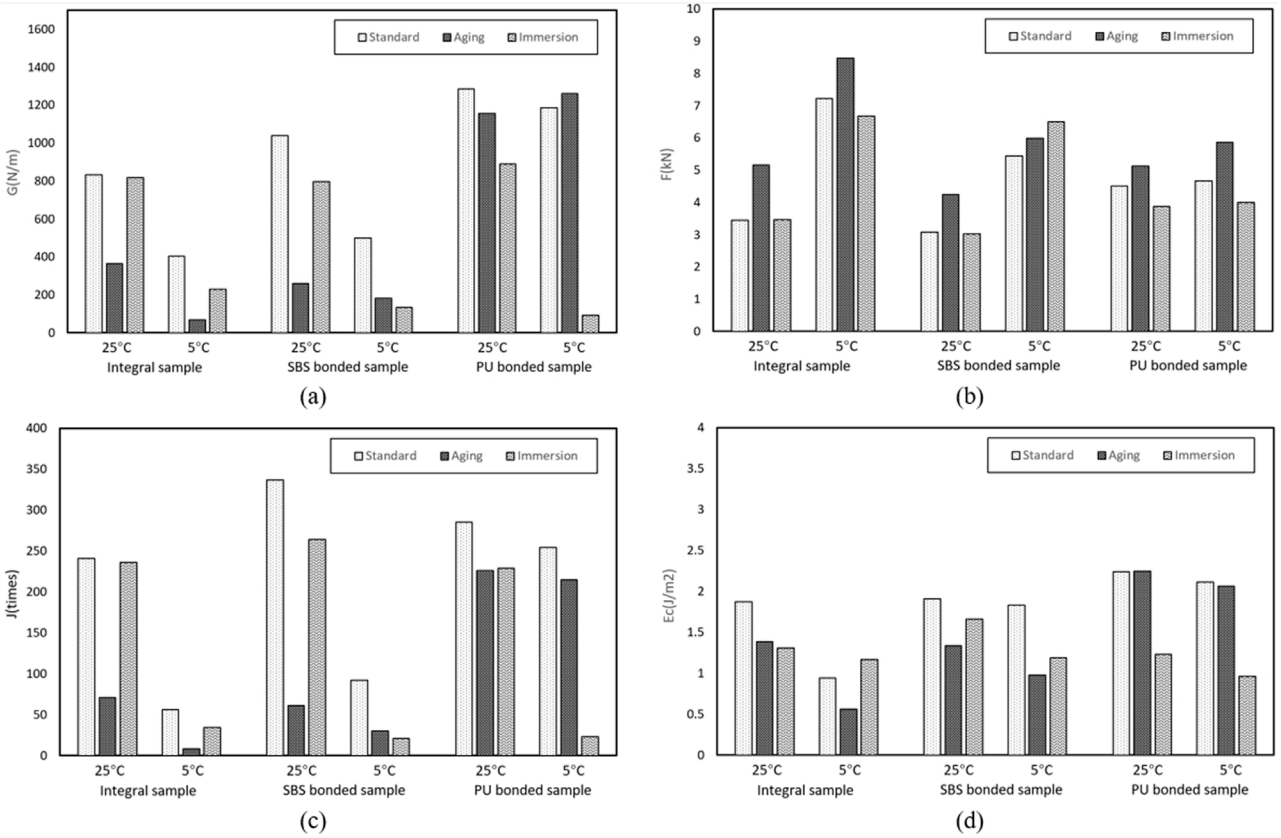

FIGURE 5
Results under different temperature conditions: **(A)** cumulative fracture energy ***G***; **(B)** maximum load of the first cycle ***F***; **(C)** allowable failure time ***J***; and **(D)** critical fracture energy ***Ec***.

fracture strain tolerance concepts, defining ***J*** as the ratio of ***G*** to ***F***. (Zhai et al., 2018).

- Average fracture energy (G^*);

G^* is defined as the ratio of ***G*** to ***N*** to remove the limitation of solely using ***G*** for evaluation.

- Critical fracture energy (***Ec***);

Ec refers to the energy required for crack propagation until fracture occurs. This parameter indicates the fracture toughness of the material.

In order to further understand the relationships between these key performance indicators and identify which factors most significantly impact crack resistance, grey correlation analysis was applied. Gray theory quantitatively compares and analyzes development trends based on the similarity or dissimilarity among factors, measuring the degree of influence between them (Liu et al., 2021). By calculating the correlation and ranking of the target value (reference series) and influencing factors (comparison series), it identifies the main factors that impact the target value. The specific method of grey relational analysis is as follows (Equations 1–5):

- Determine the reference series;

$$x_0 = \{x_0(i) \mid i = 1, 2, \cdots, n\} \tag{1}$$

- Determine the comparison series;

$$x_j = \{x_j(i) \mid i = 1, 2, \cdots, n\} (j = 1, 2, \cdots, n) \tag{2}$$

- Dimensionless processing involves dividing all numbers in the sequence by the first number in the sequence to obtain a new dimensionless sequence.
- Correlation coefficient calculation;

$$\xi_j(k) = \left| \frac{\min\limits_{j=1,n} \min\limits_{i=1,n} \Delta_j(i) + \rho \max\limits_{j=1,n} \max\limits_{i=1,n} \Delta_j(i)}{\Delta_j(i) + \rho \max\limits_{j=1,n} \max\limits_{i=1,n} \Delta_j(i)} \right| \tag{3}$$

$$\Delta_j(i) = \left| x_0(i) - x_j(i) \right| \tag{4}$$

- Correlation calculation;

$$r_j = \frac{1}{n} \sum_{i=1}^{n} \xi_j(i) \tag{5}$$

By ranking the correlation coefficients, the impact weights of various indicators on a specific road performance can be intuitively judged.

2.2.4 Experimental design

All specimen groups were tested at controlled temperatures of 25°C and 5°C (given that the specimen is prone to sudden fracture and the data becomes highly discrete when the temperature drops below 5°C, the low-temperature OT test was conducted at 5°C). In addition to standard conditions, OT specimens also underwent water immersion and long-term aging tests as specified in JTG E20-2011, respectively. Each test group consisted of 18 specimens, divided equally among three testing conditions, with three specimens per condition tested at each temperature.

- Water immersion;

Specimens were placed in a 60°C water tank and insulated for 48 h.

- Long-term aging;

Specimens were placed in an 85°C oven and continuously heated for 5 days with forced ventilation.

3 Results and discussions

As per the test plan, the results presented in the subsequent section reflect the average values of the OT tests conducted under standard, immersion, and aged conditions, as shown in Table 4.

3.1 Temperature effect

An integral part of assessing the robustness of bonding materials involves understanding the impact of temperature variations. This section delves into the temperature effect on different OT specimens, emphasizing the contrast between standard (25°C) and low-temperature (5°C) conditions.

The test results shown in Figure 5 demonstrate that at 25°C, polyurethane bonded specimens exhibit superiority in several aspects over SBS-bonded specimens in terms of parameters ***F***, ***G***, ***N***, and ***Ec***. This indicates that the polyurethane bonded samples require greater stress and energy to initiate cracks, thereby affirming the effectiveness of polyurethane grouting materials in enhancing the crack resistance properties of the mixtures.

As temperature decreases to 5°C, the stiffness of the bonding materials notably increases, which is evident in the substantial elevation of the initial load (***F***) under low temperature conditions. For example, load value for the second group of samples rises to 5.44 at low temperatures, marking a 1.77-fold increase from the value at 25°C, while the load value for the third group of samples climbs to 4.66, a 1.03-fold increase from 25°C. Despite the augmented load values suggesting that the materials can endure greater forces during initial load bearing, this does not signify an improvement in overall material performance. Instead, the heightened brittleness at lower temperatures results in a greater propensity for cracking, as demonstrated by the reduction in ***J*** and ***G***, signaling a decrease in the materials' crack resistance and durability under cold conditions.

Moreover, both immersion and aging conditions highlighted a pronounced degradation in material performance, with distinct patterns similar to those observed at low temperatures. Specifically, under water immersion at 25°C, PU and SBS bonded specimens exhibited notable decreases in ***J*** values, reflecting moisture's detrimental impact on mechanical properties. This effect was more pronounced at 5°C, where low temperatures intensified the negative impacts, particularly for PU materials, due to changes in their internal structure from the combined effects of cold and moisture. Aging further exacerbated material brittleness, significantly deteriorating material properties at 5°C. Notably, SBS materials showed a greater sensitivity to low temperatures after aging, as evidenced by the substantial declines in ***J*** and ***G*** values, indicating a heightened vulnerability under these conditions. These detailed analyses conclusively demonstrate that, across a range of conditions—be it standard, water-immersed, or aged—a decrease in temperature consistently precipitates a decline in material performance. Additionally, particular environmental factors such as immersion and aging amplify this deterioration.

3.2 Aging effect

At a standard temperature of 25°C, the impact of aging varies among different specimen groups. Observations from the first control group reveal that aging markedly enhances the brittleness of the asphalt mixture while reducing its ductility; the ***N*** value decreased from 1,200 to 297, and the ***G*** value dropped from 831.29 N/m to 365.6 N/m. These results suggest that aging precipitates both chemical reactions and physical transformations, notably triggering molecular rearrangement and a decline in adhesive properties within the binder. Furthermore, the oxidation process results in the volatilization of lighter fractions and an increase in cross-linking density within the material, thereby substantially impairing various performance metrics.

In a comparative analysis under identical aging conditions, significant disparities in performance emerged between the second and third groups. The ***R*** value of the SBS bonded specimen rises from 89.4% to 93.2%, signifying a pronounced deterioration in crack resistance throughout the aging process. Conversely, the ***R*** value for the PU bonded specimen modestly increased from 78.1% to 83.7%, underscoring the superior aging resistance of the PU material. This variance stems from the distinct chemical and physical reactions that each material undergoes during aging. The SBS material, characterized by a lower cross-linking density and a polymer structure vulnerable to thermo-oxidative effects, is more susceptible to degradation when exposed to elevated temperatures and oxygen. This vulnerability leads to diminished adhesive strength and crack resistance, thereby adversely affecting its durability under cyclic loading.

The PU material capitalizes on its high-functionality polyether groups and multi-group isocyanate linkages, providing it with exceptional resistance to oxidation and thermal aging. This configuration enables the material to maintain substantial chemical

10.3389/fbuil.2024.1443587

TABLE 4 Test results under different conditions.

Groups	Conditions		R(%)	N	G(N/m)	F(kN)	J(times)	G*(N/m)	E_C(J/m^2)
One. Integral sample	Standard	25°C	78.8	1,200	831.29	3.45	241	0.69	1.87
		5°C	93.2	149	404.5	7.22	56	2.71	0.94
	Aging	25°C	93.1	297	365.6	5.16	71	0.54	1.39
		5°C	93.2	48	66.43	8.47	8	8.30	0.56
	Immersion	25°C	90.7	1,200	817.69	3.46	236	0.68	1.31
		5°C	93.4	34	229.87	6.67	34	6.76	1.17
Two. SBS bonded sample	Standard	25°C	89.4	1,200	1,039.33	3.08	337	0.87	1.91
		5°C	93.2	168	499.36	5.44	92	11.89	1.83
	Aging	25°C	93.2	321	258.41	4.24	61	0.25	1.34
		5°C	93.2	20	181.47	5.98	30	6.05	0.98
	Immersion	25°C	91.2	1,200	795.99	3.02	264	0.66	1.66
		5°C	93.3	19	134.41	6.49	21	14.93	1.19
Three. PU bonded sample	Standard	25°C	78.1	1,200	1,283.41	4.51	285	1.07	2.24
		5°C	79.5	1,200	1,184.72	4.66	254	0.99	2.11
	Aging	25°C	83.7	1,200	1,155.48	5.12	226	0.96	2.25
		5°C	81.9	1,200	1,259.15	5.87	215	1.05	2.06
	Immersion	25°C	93.1	229	887.68	3.87	229	3.88	1.23
		5°C	93.3	28	91.96	3.99	23	3.28	0.96

and physical stability under conditions of aging. For example, the cumulative fracture energy (***G***) of PU steadily holds at 1,155.48 N/m post-aging, significantly surpassing that of SBS, which reduces to 258.41 N/m. Moreover, the load cycle (***N***) for PU consistently remains at 1,200, demonstrating its superior aging resilience. A deeper analysis of the data reveals that while both materials exhibit an increase in the initial maximum load (***F***) due to material hardening post-aging, this increase is less pronounced for the PU material. Further examination of ***J*** values illuminates the potential failure risks the materials may confront after prolonged service. The ***J*** value for PU declined from 285 to 226, yet remains considerably higher than that of SBS, which decreased from 337 to 61 (Figure 6C). This observation reinforces that PU material retains superior structural integrity and crack resistance throughout the aging process, thereby underscoring its pronounced advantage in terms of aging resistance.

3.3 Immersion effect

In the water immersion experiments, we observed significant differences in the response of various specimen materials to the water-soaked environment and drawn Figure 7 for comprehensive comparison.

Data from the first set of control specimens indicate that water immersion led to a decline in material performance; for instance, the ***R*** value increased from 78.8% to 90.7%, while the ***G*** value decreased from 831.29 N/m to 817.69 N/m. These changes suggest that water immersion may affect the cohesion within the material, thereby reducing its overall crack resistance. The penetration of water can alter the adhesive properties within the asphalt matrix, resulting in diminished bonding performance. Furthermore, the effects of water immersion are more pronounced at a lower temperature of 5°C, where the control group's ***N*** dramatically dropped to 34, indicating that lower temperatures exacerbate the negative impacts of water immersion. In such conditions, the lower temperatures intensify the internal stresses within the material, increasing the brittleness of the asphalt mix as temperatures fall. The presence of water could further weaken the bond between asphalt and aggregate, accelerating the formation and expansion of cracks, and leading to a sharp decline in performance indicators.

Under identical conditions of water immersion, there was also a notable disparity in performance between the second and third group specimens. The ***R***-value for the SBS-bonded specimens

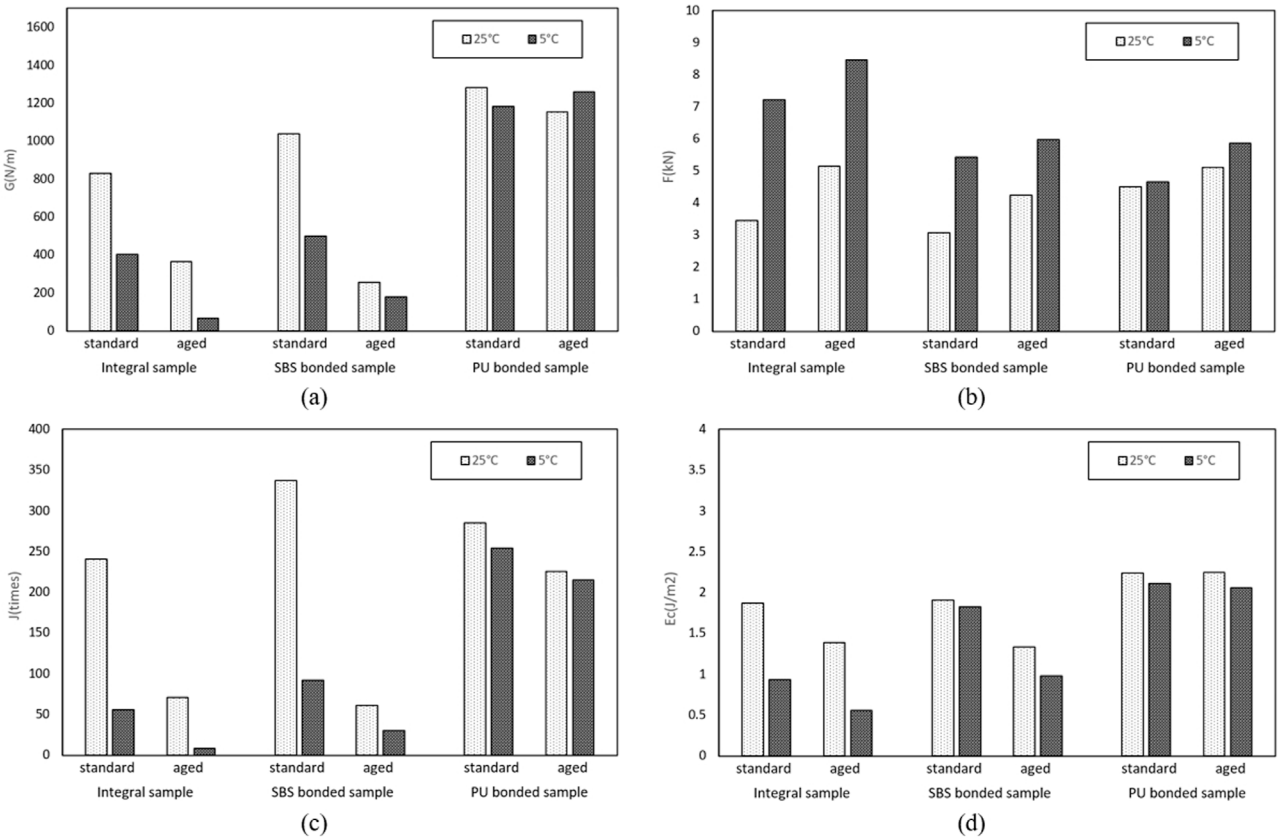

FIGURE 6
Results under different aging conditions: **(A)** cumulative fracture energy ***G***; **(B)** maximum load of the first cycle ***F***; **(C)** allowable failure time ***J***; and **(D)** critical fracture energy ***Ec***.

slightly worsened, increasing from 89.4% to 91.2%, signaling a marginal decline in crack resistance. However, this decline in crack resistance under water immersion conditions was more temperate compared to its performance under aging conditions, underscoring the enhanced stability of SBS materials against water erosion relative to the thermal oxidation effects encountered during aging. In contrast, the ***R***-value for PU-bonded specimens markedly rose from 78.1% to 93.1%, particularly in the testing environment at 5° post-immersion, where the ***N***-value precipitously dropped by 28 times, indicating a significant degradation in crack resistance under water immersion conditions, which sharply contrasts with its exhibited superior aging resistance during aging tests.

PU materials form a complex three-dimensional network structure by cross-linking the NCO groups of isocyanates with the OH groups of polyols through a polymerization reaction, theoretically enhancing chemical stability; however, significant performance degradation was observed during water immersion tests. For instance, the cumulative fracture energy (***G***) of PU decreased from 1,283.41 N/m to 887.68 N/m. Although SBS also showed a decline, it was from 1,039.33 N/m to 795.99 N/m, a lesser reduction. Moreover, the loading cycles (***N***) for PU specimens dropped dramatically from 1,200 to 229, significantly lower than the consistent performance of SBS at 1,200. Further examination revealed a decrease in the ***J*** value for PU from 285 to 229, while the ***J*** value for SBS also decreased from 337 to 264, albeit at a lesser rate. These observations emphasize the significant deterioration in the structural integrity and crack resistance of PU materials during water immersion, contrasting with their superior aging resistance shown during the aging process. This degradation is speculated to be primarily due to the hydrolysis of the urea bonds (formed by the reaction of NCO and OH) in polyurethane, particularly after prolonged water immersion. The rupture of these chemical bonds directly impacts the material's structural integrity and mechanical properties. Additionally, the penetration of water molecules causes physical expansion and softening of the material, further compromising the structural integrity of polyurethane. These changes are particularly pronounced in a water-immersed environment, especially under cold conditions, where the brittleness of polyurethane increases, thus exacerbating the decline in material performance. Therefore, despite PU's impressive performance under dry aging conditions, its performance in a water-immersed environment leaves much to be desired.

3.4 Gy correlation analysis

In this study, gray theory was employed to examine the relationships between ***N*** and the indices ***F***, ***G***, ***G****, ***J***, and ***Ec***. ***N***

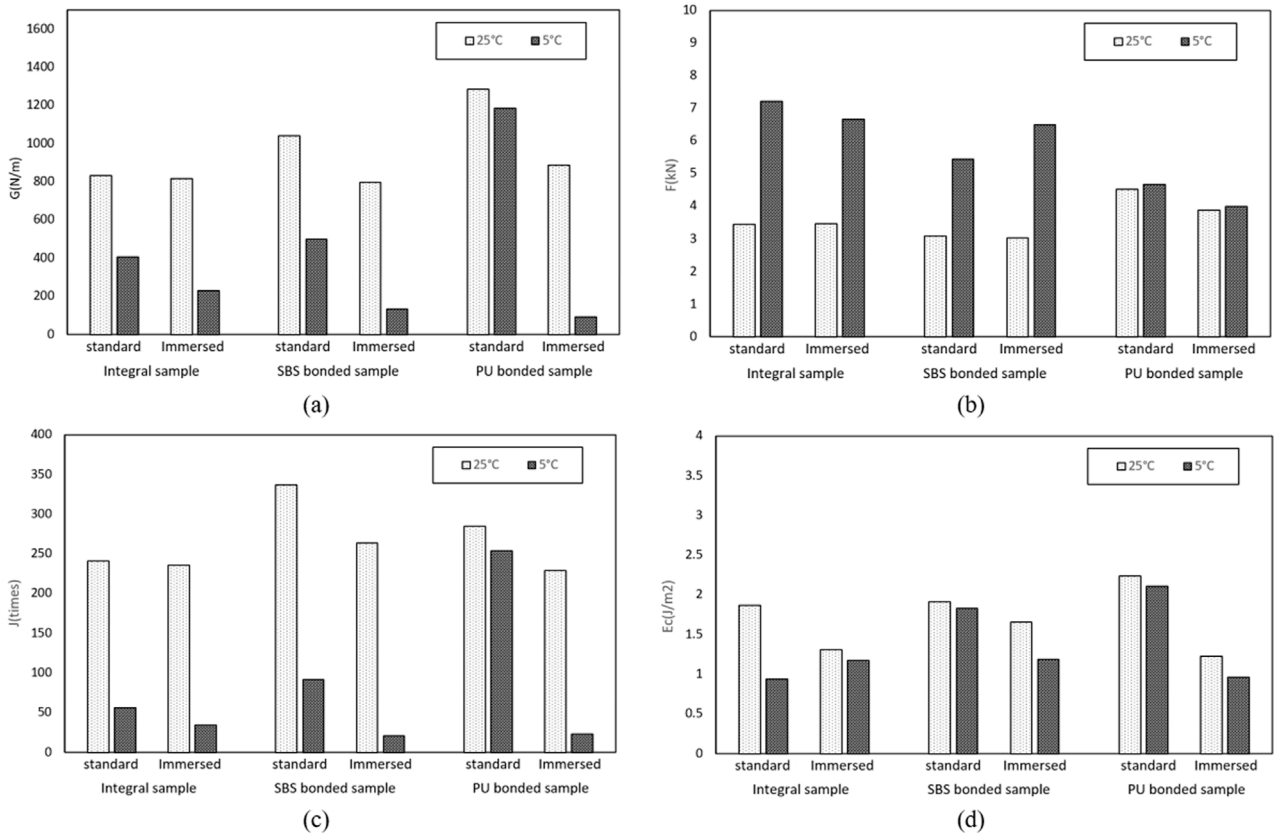

FIGURE 7
Results under different immersion conditions: **(A)** cumulative fracture energy ***G***; **(B)** maximum load of the first cycle ***F***; **(C)** allowable failure time ***J***; and **(D)** critical fracture energy ***Ec***.

TABLE 5 Gray correlation degree of each evaluation index.

Factor	G	F	J	Ec	G*
Correlation	0.7822	0.6312	0.6992	0.6033	0.5932

served as the reference sequence, while the other evaluation indices functioned as comparison sequences for the analysis.

Table 5 reveals the gray correlation degrees for each evaluation index as follows: cumulative fracture energy ***G*** > allowable failure times ***J*** > maximum load of the first cycle ***F*** > critical fracture energy ***Ec*** > average fracture energy G^*. Notably, the correlation between ***N*** and ***G*** exceeds 0.75. Both ***N*** and ***J*** serve as accurate indicators of crack resistance of adhesive bonded asphalt mixtures. ***G***, however, is only reliable when the number of loading cycles or the load loss rate is similar; otherwise, it is prone to misinterpretations. Meanwhile, ***F*** is suitable for depicting the initiation of reflective cracks and the nature of initial cracks, although it does not capture the expansion process. Evaluating the crack resistance of asphalt mixtures should not solely focus on the origins of the cracks. Overall, it is advisable to use ***N***, ***J***, and ***G*** for a comprehensive assessment of crack resistance of the bonding materials.

Although gray correlation analysis provides a powerful tool for assessing and comparing the effects of different indicators, it also has some limitations. First, the accuracy of the analysis highly depends on the quality and completeness of the data. Insufficient or biased data sampling may lead to inaccurate results in correlation analysis. Secondly, the choice of the resolution coefficient (***ρ***) used in the calculation of correlation degrees can affect the outcomes, and different resolution coefficients may lead to significant differences in correlation degrees. Therefore, an appropriate resolution coefficient should be carefully selected when applying this analysis. Moreover, gray correlation analysis can only provide the relative importance of the indicators, not establish causality, which must be clearly stated when interpreting the results.

4 Conclusion

This study conducted an evaluation of the anti-cracking performance of polyurethane grout compared to traditional SBS-modified asphalt using the Overlay Test (OT). The results indicate that under standard testing conditions at 25°C, polyurethane grout significantly enhances the crack resistance of bonded asphalt mixtures, effectively prolonging the initiation period of cracks, thereby improving the overall durability and crack propagation resistance of the mixtures. These findings highlight the potential application of polyurethane grout in modern road materials, especially in pavements requiring high durability.

However, the performance of this material under low temperatures (5°C) and water immersion conditions demonstrates certain limitations. In these extreme environments, the efficacy of polyurethane grout diminishes, particularly its crack resistance. This reduction in performance may be associated with changes in the chemical and physical properties of the material under cold and wet conditions. Nonetheless, compared to SBS-modified asphalt, polyurethane grout exhibits superior performance retention even after extensive aging, indicating its potential advantages in aging resistance.

Through grey correlation analysis, this study further quantitatively assessed the relationship between key performance indicators and the crack resistance of polyurethane grout. The analysis revealed that the order of correlation among the evaluation indices is as follows: cumulative fracture energy (***G***) > allowable failure times (***J***) > maximum load of the first cycle (***F***). Notably, the correlation between the number of loading cycles (***N***) and cumulative fracture energy (***G***) exceeds 0.75, demonstrating that these indicators are highly predictive and accurate in assessing the crack resistance of polyurethane grout.

In terms of long-term performance, the aging tests followed by regular and low-temperature evaluations clearly demonstrate that polyurethane grout exhibits superior crack resistance compared to SBS-modified asphalt, particularly under low-temperature conditions where SBS shows significant degradation. This enhanced durability, even under adverse environmental conditions, suggests that polyurethane grout could offer a more sustainable solution for pavement applications. While its initial cost is higher than that of SBS-modified asphalt, the extended durability and reduced maintenance requirements of polyurethane grout could lead to considerable cost savings over the pavement's lifecycle, making it a potentially more cost-effective option for long-term road maintenance despite the higher upfront investment.

Despite these promising results, this study has certain limitations. The performance of polyurethane grout in extreme conditions, such as prolonged low temperatures and water immersion, highlights the need for further optimization to fully harness its potential in more demanding environments. Future research should focus on refining the material's formulation and application techniques to address these limitations, aiming to expand its applicability across a broader range of environmental conditions and ensure its long-term reliability in real-world scenarios.

Data availability statement

The original contributions presented in the study are included in the article/supplementary material, further inquiries can be directed to the corresponding author.

Author contributions

KZ: Conceptualization, Methodology, Writing–original draft. HL: Data curation, Project administration, Writing–review and editing. FH: Conceptualization, Formal Analysis, Writing–review and editing. ZC: Conceptualization, Formal Analysis, Writing–review and editing.

Funding

The author(s) declare that no financial support was received for the research, authorship, and/or publication of this article.

Conflict of interest

Author KZ was employed by Shandong Hi-speed Construction Management Group Co., Ltd. Authors FH and ZC were employed by Shandong Expressway Peninsula Investment Co., Ltd.

The remaining author declares that the research was conducted in the absence of any commercial or financial relationships that could be construed as a potential conflict of interest.

Publisher's note

References

Braun, M., Fischer, C., Baumgartner, J., Hecht, M., and Varfolomeev, I. (2022). Fatigue crack initiation and propagation relation of notched specimens with welded joint characteristics. *Metals* 12, 615. doi:10.3390/met12040615

Chen, L. (2019). *Study on mechanical properties of polypropylene filament geotextile and prevention of reflective cracks*. MA thesis. Liaoning: Liaoning Technical University. doi:10.27210/d.cnki.glnju.2019.000055

Fang, N. R., Hu, S. Q., Wu, Z. Y., Sun, Y. N., and Han, J. C. (2023). Prediction method of asphalt pavement life after semi-rigid base cracking. *J. Chongqing Jiaot. Univ. Sci.* 10, 45–52. doi:10.3969/j.issn.1674-0696.2023.10.06

Gao, X., Huang, W., Wei, Y., and Zhang, Y. H. (2017). Compressive strength test and simulation of polyurethane polymer grouting materials. *Acta Mater. Compos. Sin.* 34 (2), 438–445. doi:10.13801/j.cnki.fhclxb.20160413.002

Gu, F., Luo, X., Zhang, Y. Q., and Lytton, R. L. (2015). Using overlay test to evaluate fracture properties of field-aged asphalt concrete. *Conster. Build. Mater.* 101, 1059–1068.

Hu, H. B. (2019). *Experimental study on crack resistance of reinforced cement stabilized macadam base by basalt fiber belt*. MA thesis. Xi'an: Chang'an University.

Hu, L. X. (2021). *Life prediction of asphalt overlay of old cement concrete pavement based on reflection crack*. MA thesis. Chongqing: Chongqing Jiaotong University. doi:10.27671/d.cnki.gcjtc.2021.000334

Jiang, Y., Guo, F., Kong, H., Lu, Y., and Sun, B. T. (2022). Current situation and development strategy of grouting material. *New Chem. Mater.* (01), 282–286. doi:10.19817/j.cnki.issn1006-3536.2022.01.057

Li, J., Wang, B., Zhang, J. W., and Hu, H. M. (2017). Experimental research on dynamic property of polymer grouting materials. *J. Build. Mater.* (02), 198–203. doi:10.3969/j.issn.1007-9629.2017.02.007

Liu, R. T., Zheng, Z., and Li, S. C. (2018). Mechanical properties of fractured rock mass with consideration of grouting reinforcement. *China J. Highw. Transp.* 31 (10), 284–291. doi:10.3969/j.issn.1001-7372.2018.10.028

Liu, S. F., Forrest, J., and Yang, Y. L. (2021). *Grey system theory and its applications*. 10th ed. Beijing: Science Press.

Liu, Y. J. (2019). *Polyurethane resins and their applications*. Beijing: Chemical Industry Press.

Pan, R. (2019). Performance of warm mixed rubber asphalt mixture of stress absorbing layer. *J. Chang'an Univ. Sci. Ed.* (06), 49–56. doi:10.19721/j.cnki.1671-8879.2019.06.006

Qian, J. S., Chen, X. R., Zhen, Y., and Fu, W. (2018). MMLS3-based research on anti-reflective cracking performance of geotextile. *J. Tongji Univ. Sci.* (08), 1042–1048. doi:10.11908/j.issn.0253-374x.2018.08.006

Shen, A. Q., Long, H. J., Guo, Y. C., Li, P., and Huo, C. W. (2021). Anti-cracking performance of basalt warp knitted fiber cloth based on reflection crack prevention. *Bull. Chin. Ceram. Soc.* (12), 4151–4157+4166. doi:10.16552/j.cnki.issn1001-1625.2021.12.013

Su, W. G., and Zhu, Y. (2022). Application research on active and passive anti-reflective cracks on ultra-thin asphalt overlay of cement pavement. *J. Henan Univ. Sci. Technol. Sci.* 43 (3), 55–62. doi:10.15926/j.cnki.issn1672-6871.2022.03.009

TxDOT (Texas Department of Transportation) (2021). *Overlay test*. Austin, TX: TxDOT.

Walubita, L. F., Fuentes, L., Lee, S. I., Guerrero, O., Mahmoud, E., Naik, B., et al. (2021). Correlations and preliminary validation of the laboratory monotonic overlay test (OT) data to reflective cracking performance of in-service field highway sections. *Constr. Build. Mater.* 267, 121029. doi:10.1016/j.conbuildmat.2020.121029

Wang, J., Fang, H. Y., Yu, Z. S., Cao, K., and Wang, F. M. (2019). Experimental study on uniaxial compression performance of high polymer crushed stone mixture. *J. Build. Mater.* 22 (02), 320–326. doi:10.3969/j.issn.1007-9629.2019.02.024

Wang, T. (2018). *Experimental study on the new polyurethane double liquid grouting material grouting to reinforce broken rock mass*. MA thesis. Anhui: AnHui University of Science and Technology.

Wang, X. L., Huang, X. M., and Bian, G. J. (2016). Analysis on mechanism of using LSPM for preventing reflective cracks in asphalt prevent with semi-rigid base. *J. Highw. Transp. Res. Dev.* (07), 12–18. doi:10.3969/j.issn.1002-0268.2016.07.003

Wei, J., Fu, T., and Liang, J. (2021). Fracture performance of a large-stone asphalt mixture based on a monotonic tensile overlay test. *Adv. Civ. Eng.* 6622024, 1–11. doi:10.1155/2021/6622024

Xu, C. C., Ma, N. X., Zhu, J. W., Wang, Y., and Wu, Y. F. (2024). Research on flexural performance of reinforced concrete beams strengthened with high-strength polyurethane composites. *Ind. Constr.* 54 (03), 227–236. doi:10.3724/j.gyjzg23062506

Xu, W., Zhao, S. J., Zhang, W. Z., and Zhao, X. B. (2024). Numerical simulation of crack propagation and branching behaviors in heterogeneous rock-like materials. *Buildings* 14, 158. doi:10.3390/buildings14010158

Zhai, R. X., Hao, P. W., Li, G. F., Zeng, Z. W., and Li, W. H. (2018). Anti-reflection cracking performance of asphalt mixture under freeze-thaw cycles. *J. Build. Mater.* (6), 150–154. doi:10.3969/j.issn.1007-9629.2018.06.022

Zhai, R. X., Chen, Y. M., Yu, O. H., Yuan, W. H., and Zeng, Z. W. (2017). Evaluation of cracking-resistance potential of large stone permeable asphalt mixture based on overlay tester. *J. Funct. Mater.* 48 (9), 9129–9135. doi:10.3969/j.issn.1001-9731.2017.09.023

Zhang, L., Wen, P. H., Wang, Z. H., Di, S. G., and Yin, W. Y. (2017). Advances in non-excavation grouting reinforcement materials in the road engineering. *Mater. Rep.* (21), 98–105. doi:10.11896/j.issn.1005-023X.2017.021.014